Aircraft Measurements for Understanding Air-Sea Coupling and Improving Coupled Model Predictions

Qing Wang
Meteorology Department, Naval Postgraduate School
Monterey, CA 93943
Phone: (831) 656-7716, Fax: (831) 656-3061 email: qwang@nps.edu

Award # N0001414WX20055

LONG-TERM GOAL

The long-term goal of this project is to understand the coupled air-sea processes and improve physical parameterizations of the coupled model in various large-scale forcing conditions.

OBJECTIVES

In FY14, the objectives of our analyses of the WP-3D based LASP measurements are to understand: 1) marine atmospheric boundary layer (MABL) structure and characteristics during the DYANMO/LASP field campaign; 2) influence of convection on MABL structure and the variability of atmospheric boundary layer thermodynamic properties across the DYNAMO domain during the suppressed and active phase of MJO; and 3) variability and distribution of upper ocean properties observed using the expendable probes during different phases of MJO.

APPROACH

In FY13, we made considerable analyses on the atmospheric boundary layer and the ocean miz=xed layer structure and air-ocean interface variability using the combination of dropsonde and AXBT/AXCTD data. This research is carried out further with more quantitive analyses and statistics in our FY14 efforts to help understand the variability in MABL structure and dynamics with respect to different phases of MJO. In addition to this, dropsonde data were further classified in to disturbed (under convection) and undisturbed (under no convection or clear sky) profiles. This enabled us to differentiate the role of convection to modify the MABL structure during suppressed, active and restoring phase of MJO. One of the unique aspects of LASP/DYNAMO WP-3D project was to supplement the point observations by probing the atmospheric and oceanic variability across the DYNAMO domain. Adhering to this aspect, vertical cross section of lower atmosphere was investigated using the dropsonde profiles during the suppressed and active phase of MJO. To understand the domain wide variability of upper ocean characteristics, we examined the distribution and latitudinal variability of ocean mixed layer depth (MLD), isothermal layer depth (ILD), barrier layer thickness (BLT) and thermocline depth (D20) were investigated using AXBT/AXCTD data. Water mass analysis also performed to delineate the presence of different source waters at the DYNAMO domain.

Report Documentation Page

Form Approved
OMB No. 0704-0188

1. REPORT DATE	2. REPORT TYPE	3. DATES COVERED
30 SEP 2014		**00-00-2014 to 00-00-2014**

4. TITLE AND SUBTITLE	5a. CONTRACT NUMBER
Aircraft Measurements for Understanding Air-Sea Coupling and Improving Coupled Model Predictions	5b. GRANT NUMBER
	5c. PROGRAM ELEMENT NUMBER
6. AUTHOR(S)	5d. PROJECT NUMBER
	5e. TASK NUMBER
	5f. WORK UNIT NUMBER
7. PERFORMING ORGANIZATION NAME(S) AND ADDRESS(ES) **Naval Postgraduate School (NPS),Department of Meteorology,Monterey,CA,93943**	8. PERFORMING ORGANIZATION REPORT NUMBER
9. SPONSORING/MONITORING AGENCY NAME(S) AND ADDRESS(ES)	10. SPONSOR/MONITOR'S ACRONYM(S)
	11. SPONSOR/MONITOR'S REPORT NUMBER(S)

12. DISTRIBUTION/AVAILABILITY STATEMENT
Approved for public release; distribution unlimited

13. SUPPLEMENTARY NOTES

14. ABSTRACT

15. SUBJECT TERMS

16. SECURITY CLASSIFICATION OF:			17. LIMITATION OF ABSTRACT	18. NUMBER OF PAGES	19a. NAME OF RESPONSIBLE PERSON
a. REPORT **unclassified**	b. ABSTRACT **unclassified**	c. THIS PAGE **unclassified**	**Same as Report (SAR)**	**13**	

Qing Wang is responsible for the overall WP-3D LASP project. Analyses of the LASP/DYNAMO data were also performed by NRC postdoc Denny Alappattu.

WORK COMPLETED

Specific works done in FY2014 are listed in the following.

1. Typical structures of MABL observed during the DYNAMO/LASP were studied using the dropsonde data. Different MABL layers, including mixed or subcloud layer, transition layer, cloud layer, and trade wind inversion layer were identified.
2. Differences in the vertical cross section of MABL across the DYNAMO domain were studied in the suppressed and active phase of MJO. This analysis revealed the latitudinal variability of virtual potential temperature, specific humidity and wind in the DYNAMO domain.
3. Dropsonde soundings were separated as taken under convective and non-convective conditions comparing the probe drop location with contemporaneous METEOSAT-7 visible imagery. Resulting classification showed differences in the response of MABL under convection and no convection conditions during different phases of MJO.
4. Studied the distribution Ocean mixed layer depth (MLD), isothermal layer (ILD) and barrier layer thickness (BLT) with respect to the different phases of MJO.
5. Latitudinal variability of thermocline depth, isothermal depth and mixed layer depth in response to the MJO cycle were investigated.
6. Water mass analysis was performed using the AXCTD temperature, salinity and density profiles to identify source waters present during the active phase of MJO.
7. Analyses of aircraft in situ measurements for precipitating cumulus-topped boundary layers and for precipitating deep cumulus topped boundary layers.

RESULTS

MABL characteristics: A total of 468 dropsondes were deployed in 12 research flights during the DYNAMO/LASP. Quality controlled dropsonde data were then used to study the thermodynamic structure and variability of MABL. Figures 1a-c show the three principal types of MABL profiles of virtual potential temperature (θ_v), equivalent potential temperature (θ_e), saturated equivalent potential temperature (θ_{es}) and specific humidity (q) observed during DYNAMO. Figure 1a is an example of the typical undisturbed trade wind cumulus tropical MABL structure. This sounding was made on 08 December 2011 at 0458Z from at 5.77°S, 72.41°E. Turbulent mixing uniformly distributes θ_v, θ_e, and q in the lowest few hundreds of meters known as mixed layer or subcloud layer. Mixed layer top can be identified by the sharp gradient in θ_v, θ_e, and q at ~540 m. Virtual potential temperature follows dry adiabatic lapse rate in the mixed layer. The inversion at the mixed layer top is the transition layer also known as entrainment zone and has a width of 240 m. Stable stratification in the transition layer impedes the turbulent updrafts from reaching the cloud layer and hence traps moisture, aerosols and other tracers in the mixed layer. Because of this, specific humidity of mixed layer is higher than the layers above. Cloud layer varied from the top of transition layer to ~ 2750 m. Negative vertical gradients of θ_e and θ_{es} in the cloud layer indicates a region of the convective instability with respect to saturated parcel displacements and conditionally unstable atmosphere. Trade wind inversion (TWI)

caps the cloud layer. TWI layer has a thickness of 280 m. This layer is formed due to the subsidence of the air in the descending limb of the Hadley cell circulation. Absence of this subsidence is the reason for the lack of TWI in MABL structure in the vicinity of Inter tropical convergence zone (ITCZ). Average TWI height during the DYNAMO was 2600 m. Observations from tropical Atlantic and Pacific oceans have shown that the TWI depths tend to be more or less horizontally uniform near 2000 m (Augstein et al. 1974). But large spatio-temporal variability in TWI has been reported from the tropical Indian Ocean (Alappattu and Kunhikrishnan 2010). Only ~5% of DYANMO soundings exhibited the well delineated TWI. This is mainly due to (1) persisted ITCZ in the DYANMO domain during the suppressed phase of MJO and (2) organized convection and disturbed condition during the active phase of MJO. So the more common structure of undisturbed clear sky MABL observed during the DYNAMO was without TWI as shown in Figure 1b. This sounding is taken on 13 November 2011 during 1153Z at (5.46°S, 74.48°E). The mixed layer depth was 631 m, and was capped by the transition layer of 289 m width. Unlike the typical MABL profiles (Figure 1a), cloud layer and TWI is not obvious in this case. Typical disturbed condition profile under strong convection observed on 28 November 2011 during 0902Z at (9.31°S, 75.09°E) is shown in Figure 1c. Layered structure could not be identified from this stable MABL profile.

Vertical cross section of MABL in the suppressed and active phase of MJO: Variability of MABL thermodynamic structure across the DYNAMO domain during the suppressed and active phase of MJO was studied using the dropsonde data. For the purpose of comparison we considered two days- 13 November and 24 November- representing the suppressed and active phase of MJO2. Conditions typical to the suppressed phase (undisturbed condition with light winds and positive SST anomaly) and active phase (disturbed condition with strong WWB and negative SST anomaly) were prevailed respectively on 13 and 24 November. Figures 2a-i shows the vertical cross section of θ_v, q and zonal wind (u) as well as corresponding mean profiles (shaded regions in the mean profiles corresponds to one standard deviation of the data) plotted using the dropsonde data taken on 13 and 24 November. These contours and mean profiles were created using 31 (13 November) and 21 (24 November) soundings made along the Diego Garcia (DG; 7.31°S, 72.42°E) to RV Revelle (RV; 0.12°N, 80.50°E) transect. Distance from DG to RV is given in the lower X axis and corresponding latitudes are shown in the upper X axis (Figures 2a and 2b). Mean mixed layer depths on 13 and 24 November were 575 m and 400 m respectively. Average mixed layer cooling observed in θ_v (Figures 1a-b) due to the transition from suppressed phase (13 November) to active phase (24 November) of MJO was ~1.5K. θ_v reduction was stronger (> 2K) towards lower latitudes, possibly due to the enhanced MJO signal in the lower latitudes. But above mixed layer, θ_v was slightly warmer on 24 November in comparison to 13 November, which is obvious in the mean profiles shown in Figure 2c. Mean θ_v profile on 24 November was slightly stable, characteristic of convective condition. Distance-height cross section of specific humidity on 13 and 24 November between DG and RV is shown in Figures 1d and 1e respectively. Compared to suppressed phase, MABL is more humid in the active phase. Average increase of ~ 1.5 g kg^{-1} specific humidity was observed in the entire MABL (Figure 1f). Characteristics of mean θ_v and q profiles observed on 13 and 24 November is similar to the undisturbed and disturbed structure of MABL reported from the central equatorial pacific (Firestone and Albrecht, 1986). Striking feature in Figures 2d and 2f is the dry layer above mixed layer in the high latitudes (nearer to DG). Marked difference in the dry layer can observed between 13 and 24 November and a detached minimum in humidity were observed in the height region between 1250 m and 1750 m on 24 November. Similar drying associated with MJO is observed during the TOGA-COARE (Johnson et al. 2001). Zonal wind changed considerably in the MABL with the onset of WWB during the active phase of MJO. Figures 2g and 2h show the zonal wind along the DG to RV transect taken on 13 and 24 November. There were no significant changes in the meridional wind between 13 and 24 November (not shown). Zonal

wind was low on 13 November and DG (RV) side was dominated by easterlies (westerlies). Onset of WWB is obvious from the Figure 2h with magnitudes exceeding 18 m/s in the MABL between ~3°S and 1°S.

Influence of convection on MABL structure: In addition to the MJO phase based classification, The DYANMO soundings were further categorized as disturbed or undisturbed soundings by comparing contemporaneous METEOSAT-7 satellite visible imagery and the soundings. Drops made in areas completely covered by high cloud tops were classified as disturbed. 54% of the soundings from the north of 10°S fall under the undisturbed category. As expected undisturbed (81%) and disturbed (63%) soundings dominated respectively in the suppressed and active phase of MJO. In the restoring phase, undisturbed (52%) and disturbed (48%) profiles distribution was approximately equal.

Mean undisturbed profiles of θ_v, q and u in the different phases of MJO are shown in Figures 3a-c. Below 2000 m, no significant difference is observed among the θ_v profiles, apart from a slightly warmer restoring phase. Mixed layer depths were comparable in the three phases. Moisture structure shows significant variability in the mixed layer with respect to the phase of MJO. While the mixed layer q remained more or less equal during suppressed and active phases, restoring phase q was ~1g/kg higher in the mixed layer. It is interesting to note here that, above mixed layer, q is higher in the suppressed phase than active phase of MJO. q was as high 10 g/kg at ~2500 m in suppressed phase. This is probably due to the enhanced shallow cumulus activity involving the vertical convective transport of moisture thereby preconditioning the atmosphere for the onset of MJO (Benedict and Randall, 2007). Active phase undisturbed condition shallow cumulus activity is low in comparison to suppressed phase as indicated by the q profile. It may be noted that the active phase of MJO is dominated by mesoscale organized convection, categorized as the disturbed condition for this study. Mean u profiles systematically increased from suppressed to restoring phase. Very low easterlies prevailed in the suppressed phase. Active phase and restoring phase was characterized by strong westerlies.

Mean disturbed condition profiles are shown in Figures 4a-c. Mean disturbed θ_v profile (Figure 4a) was the coolest during the suppressed phase of the MJO. Mean mixed layer θ_v in the suppressed phase was cooler by 1.1K (1.5K) with respect to the active phase (restoring phase) of MJO. A comparison of Figures 3a and 4a shows that MABL is potentially cooler under convective condition. MABL cooling under convective condition is due to the cold pool air. Cold pool is a region of relatively cold air surrounded by warmer air. Precipitation-induced cold pools are formed due to the cooling of the air by rainfall evaporation. Figure 4a indicates the degree of evaporative cooling is not the same for different MJO phases. While a shallow mixed layer can be identified from the suppressed phase mean θ_v profile active and restoring phase profiles were slightly stable. Suppressed phase mixed layer was also drier than other two phases under disturbed condition. But above 1000 m, q profiles were more or less equal. The u wind was westerly below ~ 1250 m and easterlies above and of very low magnitude in the suppressed phase. Wind during the active phase was dominated by strong westerlies but mean u was lower than restoring phase. In the restoring phase, u showed a double peak structure with maxima in u at ~ 800 m and ~ 3000 m.

Distribution Ocean Mixed layer, isothermal layer, barrier layer variability: Using temperature (AXCTD and AXBT) and density (AXCTD only) profiles, isothermal layer depth (ILD) and mixed layer depth (MLD) were calculated using the threshold method as defined by Sprintall and Tomczak (1992). The AXCTD and AXBT data are linearly interpolated to a vertical resolution of 0.5 m. The ILD is defined as the depth where the temperature is lower by 0.5°C from that at 10m depth. Using

AXCTD derived density profile, MLD is calculated in terms of a depth where the density is equal to the density at 10 m plus the increment in density equivalent to 0.5°C. Density increment is determined by the coefficient of thermal expansion. Temperature and salinity at 10 m is used for the computation of coefficient of thermal expansion. The difference of ILD and MLD is defined as the BLT.

Histogram of MLD during the suppressed and active phase is shown in Figures 5a and 5b. Only 14 good AXCTD profiles were available for the restoring phase. This number is inadequate to produce a meaningful statistics and hence not shown here. Suppressed phase MLD exhibit a more or less uniform distribution between 25 m to 50 m class range, with local minima around 35-40 m. MLD in the active phase had the bimodal distribution. 65% of the observation is in the 25 to 45 class mode. The mean MLD in this mode was ~ 34 m. Approximately 25% of observed MLD falls in the 60-80 m mode and the mean of this mode was ~ 65 m.

A large percentage (~80%) of ILD falls in the 25 to 60 m class range during the suppressed phase (Figure 6a). Mean suppressed phase ILD was 49 m. Active phase ILD has a mode in 25-60 m class range, similar to the suppressed phase. But there exists another mode of ILD variability in the 60-80 m class range. Thus MLD as well as ILD had the bimodal distribution during the active phase of MJO. ILD deepening during the active MJO is attributed to the strong wind and convection. During restoring phase ILD exhibited a near-normal distribution with peak in the 55-60 m class range. Mean ILD in the restoring phase (~59 m) was higher than the suppressed (mean ILD = 49 m) and active phase (mean ILD=54 m). Wind induced mixing is the primary reason for the deepening of the ILD in the restoring phase. It may be noted here that atmospheric boundary layer winds was stronger in the restoring phase in comparison with the suppressed and active phase of MJO. BLT distribution in suppressed and active phase is shown in Figures 7a and b. Irrespective of the phase of the MJO; more than half of the occurrence of BLT falls in the 0 -10 m class. Cronin and McPhaden (2002) noticed that, western pacific warm pool BL erodes in the event of WWB associated with MJO, due to the wind induced and convective mixing from surface cooling. BL thinning or annihilation during the active phase of MJO was not obvious from this particular data set. Instead, the BLT distribution exhibited a small percentage (~15%) of occurrences of thicker (> 30 m) BL during active phase.

Latitudinal Variability of thermocline depth, isothermal depth and mixed layer depth: The latitudinal variability of thermocline depth (D20) as represented by the topography of 20°C isotherm, ILD and MLD are shown in Figure 8a-c. Observations show strong latitudinal dependence of D20 variability in the suppressed, active and restoring phase of MJO. In general, D20s were high at ~ 8°S. The local minima of D20s were observed in between 4°S and 2°S, caused by the upwelling in Seychelles-Chagos thermocline ridge (SCTR). ILD variability was independent of latitude. But large scatter was observed at south of 6°S and north of 2°S. MLD variability did not show any latitude dependence.

Water mass analysis: Figures 9a-c show the T-S diagram from the AXCTD profiles taken along the DG to RV transect. Contours in the figure represent the constant potential density surfaces. Figure 9a shows the T-S diagram of ACTD profile taken ~200 km from DG. In the figure the Indonesian through flow (ITF) water can be identified as the isohaline (~35 psu) layer that present between potential densities 23.5 kg m^{-3} and 25.5 kg m^{-3}. Surface water in this region was formed by fresher tropical surface water (TSW) with a lower salinity than ITF water. TSW was also observed in the surface waters of the next three profiles (approximately 400 km (black), 600 km (blue) and 800 km (red) from DG) shown in Figure 9b. Near RV, the isohaline character of ITF is disturbed by the higher salinity water from lower latitudes. High salinity water intrusion into subsurface layers with a high salinity core at 80 m was also evident in the vertical cross section of salinity between 400 km and 800 km from

DG (not shown). This intrusion increases with decreasing latitude as seen from the red curve in Figure 10b with slightly higher salinity than other two profiles. The source of this high salinity core is water from the Arabian Sea usually referred as Arabian Sea high saline water (ASHSW).

ASHSW, identified by its characteristic high salinity, completely replaced the ITF in the two northernmost profiles closest to RV shown in Figure 9c. In comparison with the other profiles at higher latitudes, the surface water of these two profiles had different characteristic than that of TSW. Here the surface salinity was in between fresh TSW and high saline ASHSW. This is a mixture of Bay of Bengal (BoB) water and ITF.

IMPACT/APPLICATIONS

TRANSITIONS

The results from this year's research, especially the quality controlled AXBT/AXCTD datasets can be used for coupled model evaluation and diagnoses and identify model deficiencies for future improvements.

RELATED PROJECTS

None.

REFERENCES

Alappattu., D. P., P.K. Kunhikrishnan, 2010: Observations of the thermodynamic structure of marine atmospheric boundary layer over Bay of Bengal, Northern Indian Ocean and Arabian Sea during premonsoon period. *Journal of Atmospheric and Solar-Terrestrial Physics* **72**:17, 1318-1326.

Augstein, E., H. Schmidt, and F. Ostapoff, 1974: The vertical structure of the atmospheric boundary layer in undisturbed trade winds over the Atlantic. *Bound.-Layer Meteor*, **6,** 129–150.

Benedict, J. J., and D. A. Randall, 2007: Observed Characteristics of the MJO Relative to Maximum Rainfall. *Journal of the Atmospheric Sciences*, **64**, 2332-2354.

Cronin, M., and M. McPhaden, 2002: Barrier layer formation during westerly wind bursts. *J. Geophys. Res.*, **107** (C12), 2101–2112.

Firestone, J. K., and B. A. Albrecht, 1986: The structure of the atmospheric boundary layer in the central equatorial Pacific during January and February of FGGE. *Mon. Wea. Rev*, **114,** 2219–2231.

Johnson, R. H., P. E. Ciesielski, and J. A. Cotturone, 2001: Multiscale Variability of the Atmospheric Mixed Layer over the Western Pacific Warm Pool. *J. Atmos. Sci.*, **58**, 2729–2750

Sprintall, J., and M. Tomczak, 1992: Evidence of the barrier layer in the surface layer of the tropics. J. Geophys. Res., **97 (C5)**, 7305–7316.

PUBLICATIONS

1. Denny P. Alappattu and Qing Wang, (2014) Correction of depth bias in upper ocean temperature and salinity profiling measurements, accepted by *J. Atmo. Ocean. Tech.*

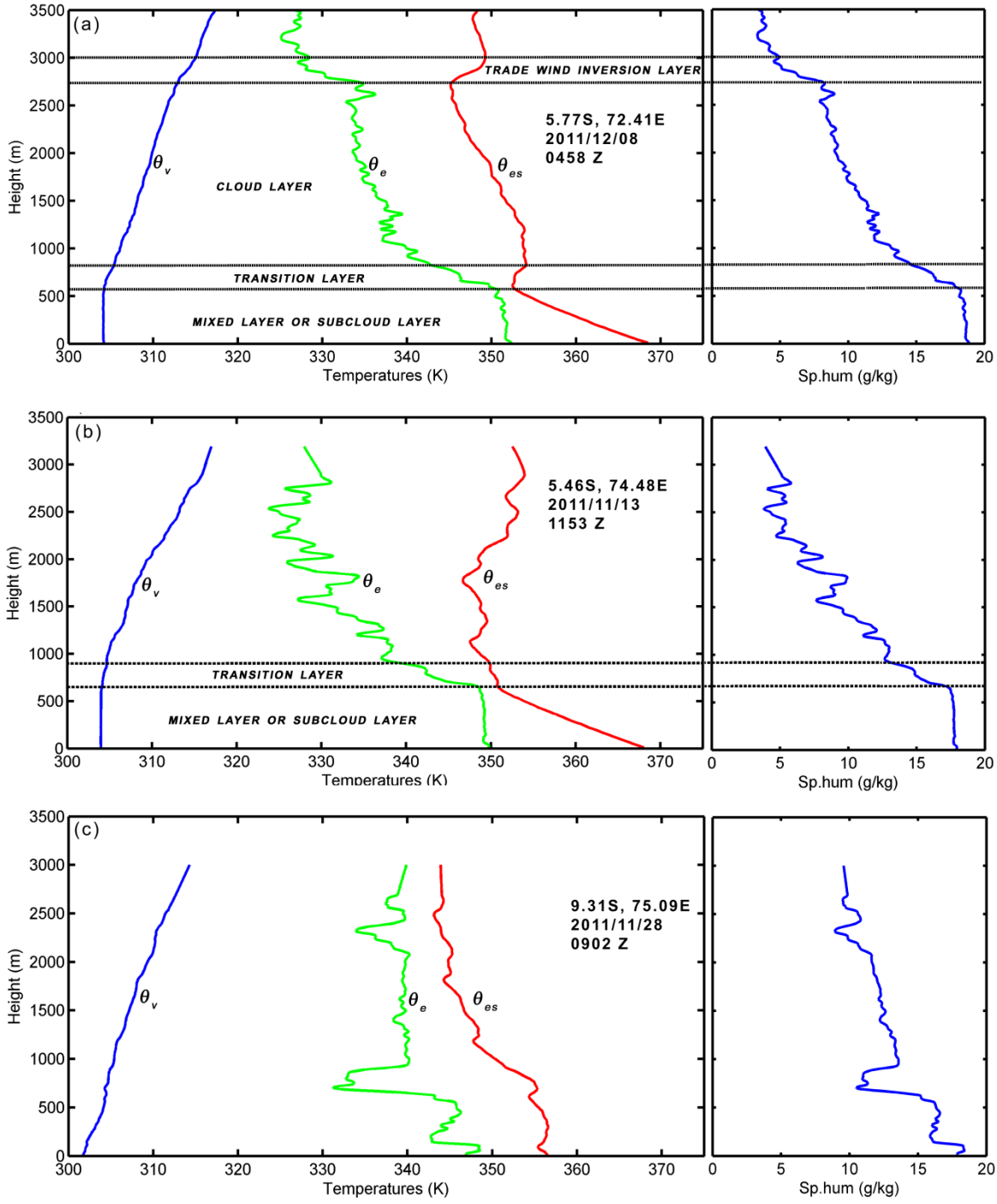

Figure 1: Typical profiles of θ_v, θ_e, θ_{es} and specific humidity under (a) undisturbed condition, (b) undisturbed condition but without trade wind inversion and (c) disturbed condition.

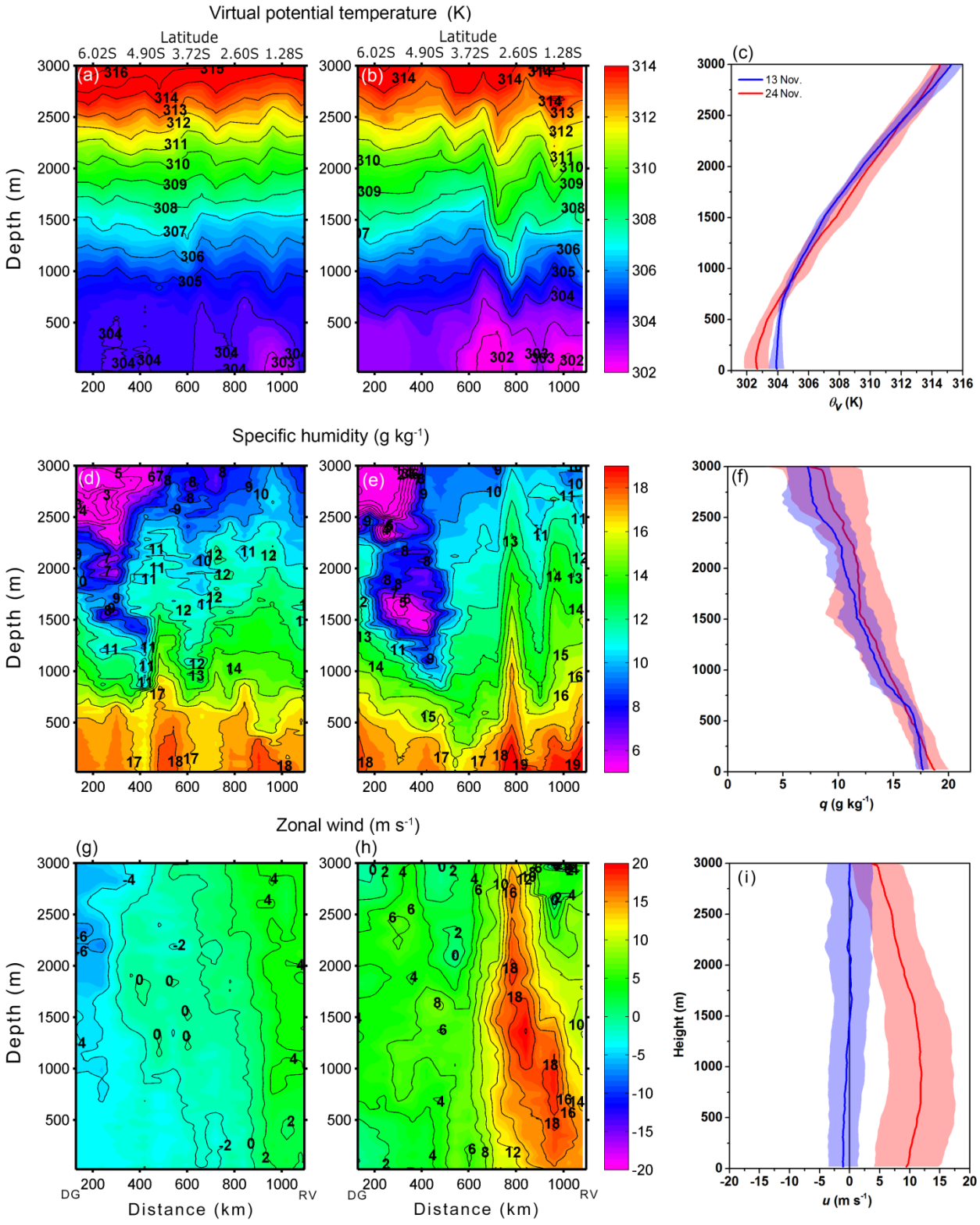

Figure 2: Vertical cross sections of virtual potential temperature, specific humidity and zonal wind along Digeo Garcia to R/V Revelle transect taken on (a, d, g) 13 November 2011, (b, e, h) 24 November 2011 and (c, f, i) corresponding mean profiles.

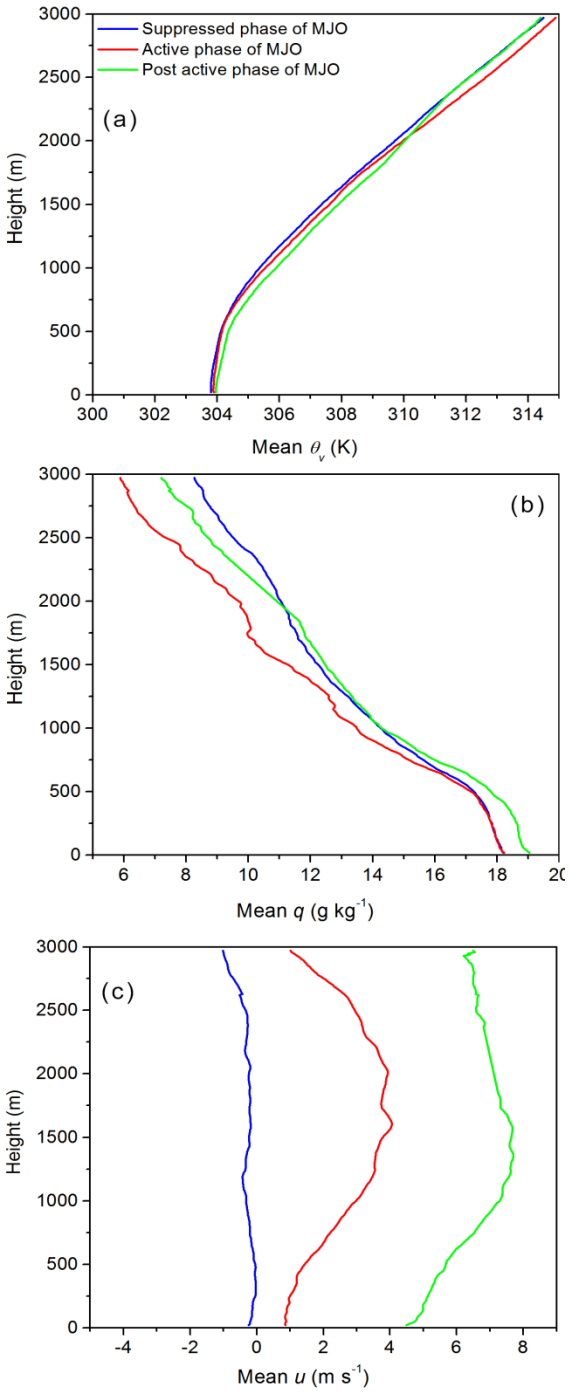

Figure 3: Vertical profiles of (a) virtual potential temperature, (b) specific humidity and (c) zonal wind under undisturbed condition.

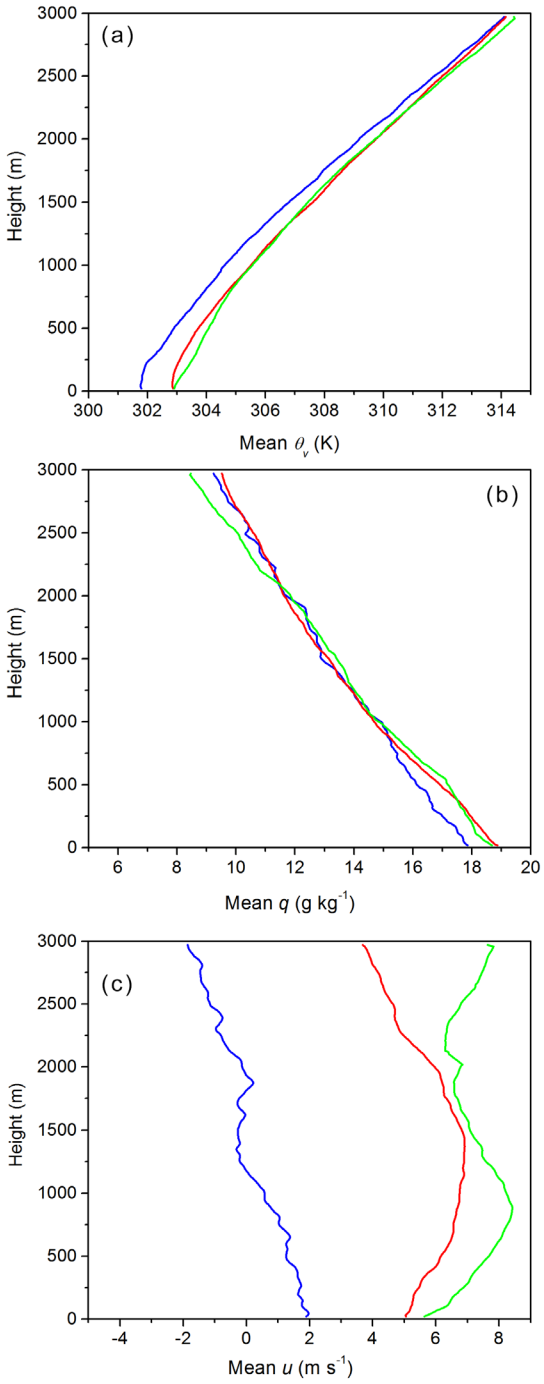

Figure 4: Same as Figure 3 but for under disturbed condition.

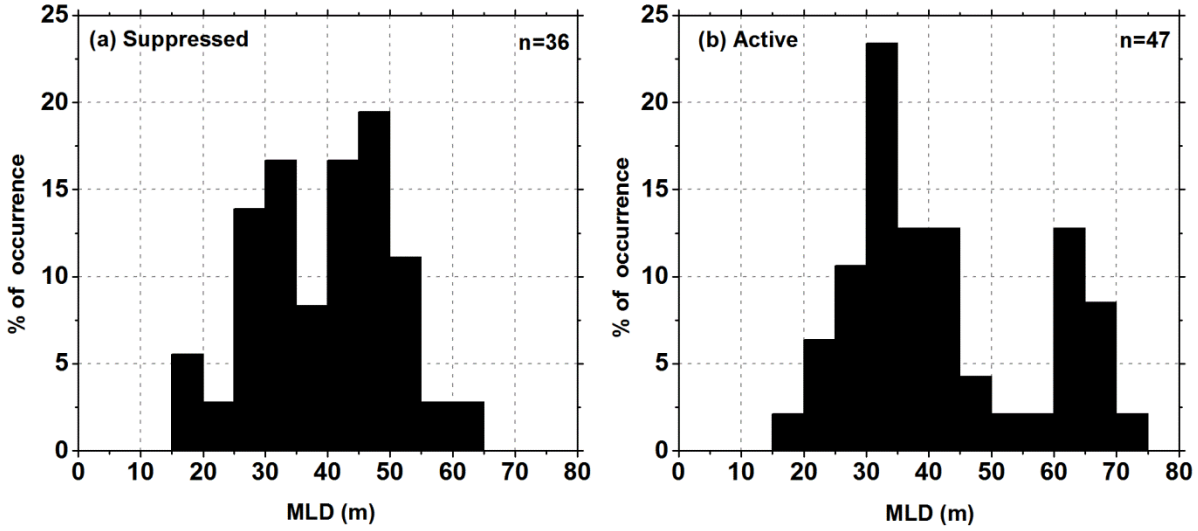

Figure 5: Distribution of mixed layer depth during (a) suppressed phase and (b) active phase of MJO.

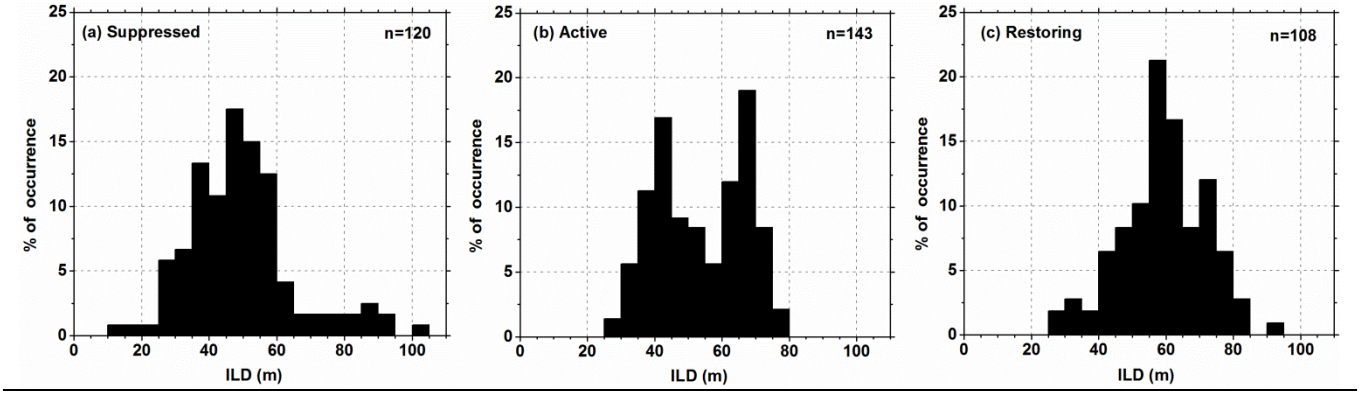

Figure 6: Distribution of isothermal layer depth during (a) suppressed phase (b) active phase and (c) restoring phase of MJO

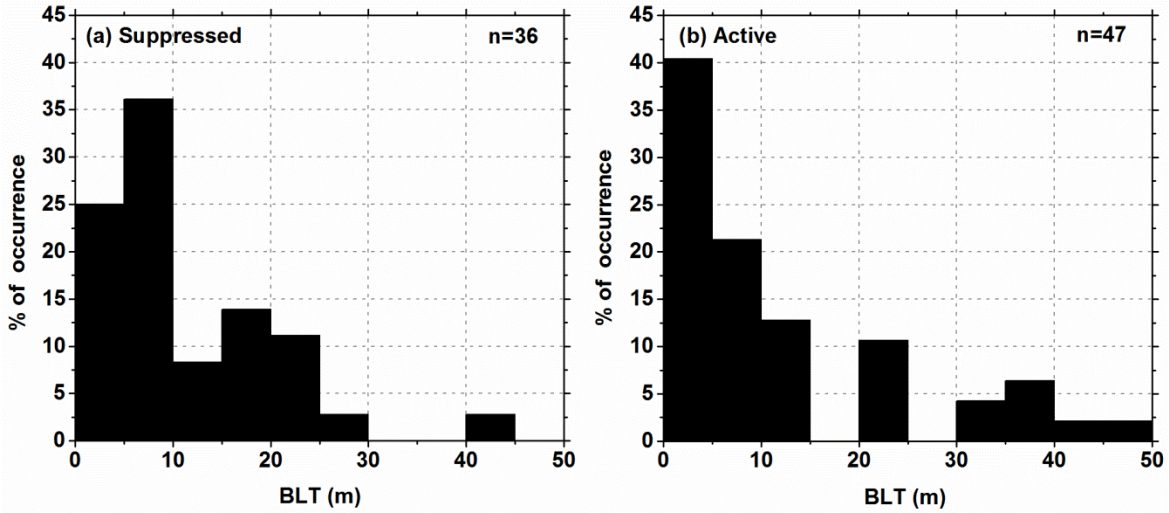

Figure 7: Distribution of barrier layer thickness during (a) suppressed phase and (b) active phase of MJO.

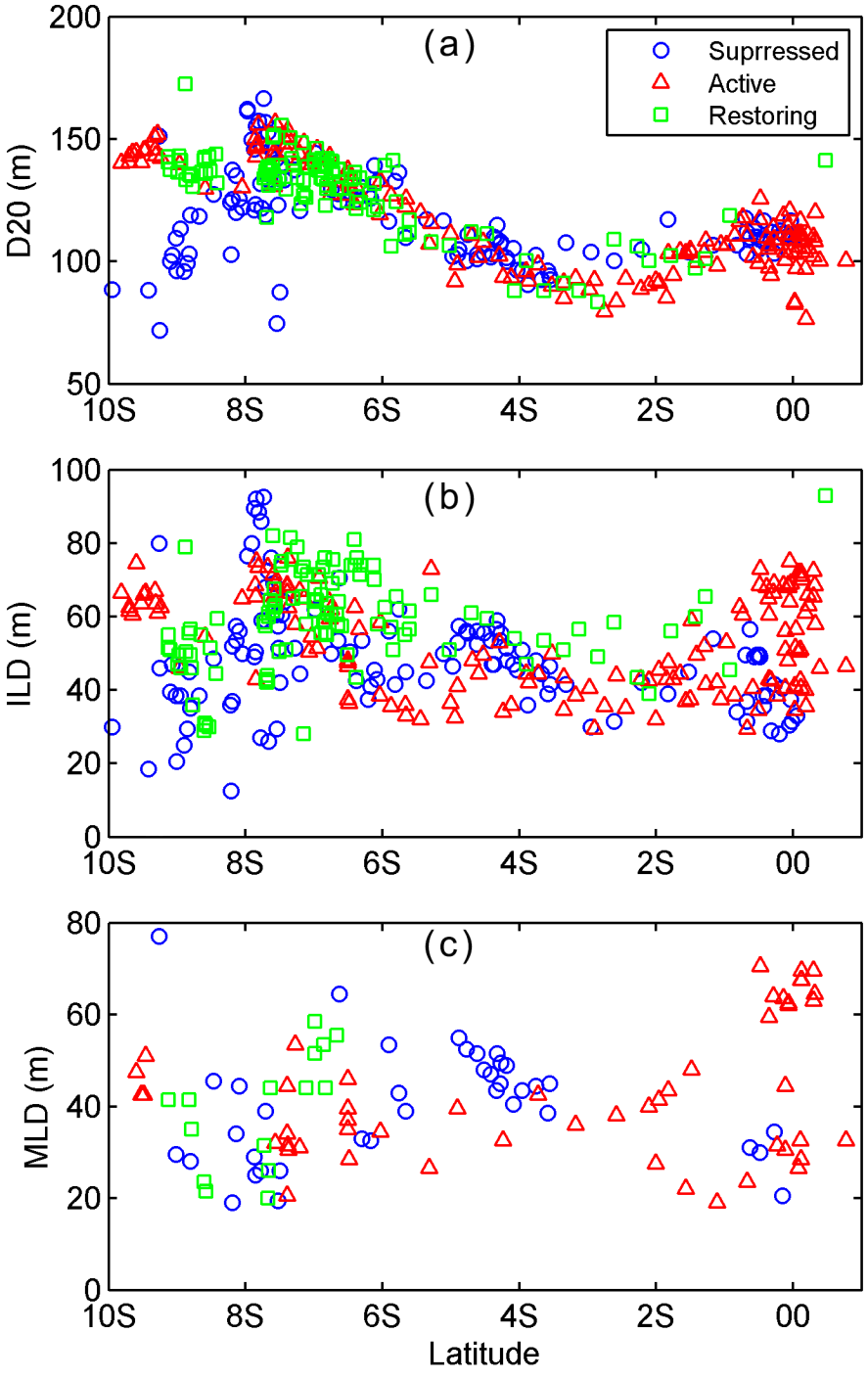

Figure 8: Latitudinal variability of (a) thermocline depth (b) isothermal layer depth and (c) mixed layer depth.

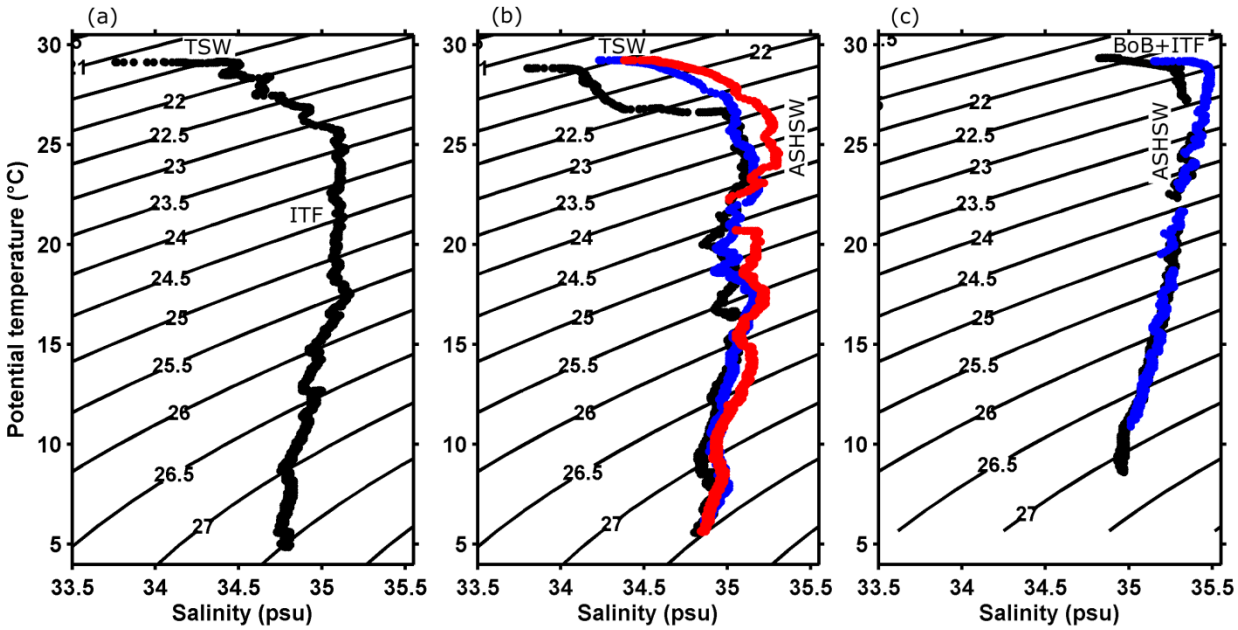

Figure 9: T-S diagrams of AXCTD profiles along DG to RV transect (a): Southernmost profile 200 km from DG. (b): Profiles 400 km (black), 600 km (blue) and 800 km (red) from DG. (c): Profile 1000 km from DG (black) and nearest to RV (blue).